19

Dispersion of Surface Plasmon-Polaritons in Metallic Single-Walled Carbon Nanotubes and Ordered Arrays Based on Them

© S.A. Afanasyev[1], V.A. Zaitsev[1], S.G. Moiseev[1,2], I.A. Rozhleys[1], D.G. Sannikov[1,¶]

[1] Ulyanovsk State University, Ulyanovsk, Russia
[2] Kotelnikov Institute of Radio Engineering and Electronics of the of the Russian Academy of Sciences, Ulyanovsk, Russia
¶ e-mail: sannikov-dg@yandex.ru

Received February 19, 2025
Revised February 19, 2025
Accepted June 30, 2025

Within the framework of a hydrodynamic model, the propagation of eigenwaves (surface plasmon-polaritons) in individual metallic single-walled carbon nanotubes (SWCNTs) and ordered arrays based on them is considered. Numerical analysis of the dispersion properties of surface plasmon-polaritons in the terahertz range is performed taking into account losses and the tensor nature of the surface conductivity of single-walled carbon nanotubes. Conditions are determined under which the interaction of neighboring nanotubes in the array does not affect the dispersion characteristics of surface plasmon-polaritons. It is shown that the highest values (over 100) of the slowing-down factor (the ratio of the speed of light to the phase velocity of surface plasmon-polaritons) of the fundamental mode are achieved for ordered arrays of single-walled carbon nanotubes with radii over 2 nm at frequencies around 40 THz and above. The results obtained may find practical application in compact amplifiers and terahertz radiation generators implemented on the basis of arrays of single-walled carbon nanotubes.

Keywords: surface plasmon-polaritons, single-walled carbon nanotubes.

DOI: 10.61011/EOS.2025.07.61909.7624-25

Introduction

Thanks to the unique combination of small size and high electrical conductivity, carbon nanotubes (CNTs) are a promising material for electronics, nanophotonics, and nanoplasmonics [1–6]. CNTs can be single or multi-walled, and depending on their conductivity type, metallic or semiconducting. It has been shown in [1,7–12] that CNTs can be treated as a plasmonic waveguide that supports the propagation of ultra-slow surface plasmon-polaritons (SPPs) with a slowing-down factor (the ratio of the speed of light to the phase velocity of SPPs) greater than 100. The phase velocity of such plasmon waves is significantly less than the speed of electromagnetic waves in free space and is comparable to the drift velocity of charge carriers in graphene $(0.5-1)\cdot 10^6$ m/s [13,14]. If the phase velocity of slowed-down SPPs and the drift velocity of charge carriers on the CNT walls are close in magnitude and coincide in direction, a drift current flowing through the nanotube can amplify the SPP wave [11,12,15.17]. In paper [18] it was proposed to use slowed-down SPPs in a terahertz radiation generator scheme based on an array of parallel double-walled CNTs carrying a direct current acting as a pump.

To describe plasmonic properties of single-walled carbon nanotubes (SWCNTs), both classical and quantum approaches can be used [6,19,20]. It is worth noting certain advantages of the classical hydrodynamic approach, within which the wall of the CNT is modeled as an infinitely thin cylindrical shell, and the valence electrons uniformly distributed over the surface of the wall interact with the electromagnetic wave and are considered as a charged fluid [21–25]. In the case of plasmon oscillations, the hydrodynamic approach allows obtaining results more simply and with less computational cost, which well agree with conclusions of semiclassical and quantum models [1,6,19].

In the present work, a numerical analysis of the dispersion characteristics of SPPs in metallic SWCNTs and in ordered arrays based on them is conducted. For a single SWCNT, within the framework of the linearized hydrodynamic model, the conductivity tensor is found, and then the determinant dispersion equation for SPPs is numerically solved, which is obtained by solving the waveguide problem of classical electrodynamics. A comparison is made with similar results obtained by computer simulation of the SPP propagation process in ordered arrays of SWCNTs. The influence of the array structure period on the dispersion characteristics of SPPs is studied.

Problem Statement. Conductivity Tensor of SWCNTs

An SWCNT is a cylindrical surface formed by carbon atoms with diameter from fractions to several nanometers and length from micrometers to hundreds of micrometers or more [26]. The SWCNT wall is conductive and characterized by surface conductivity, which in general is a tensor value. To find the conditions for the propagation of SPPs in SWCNTs, a linearized hydrodynamic theory is used (for example, see [8,22]). The problem is solved in cylindrical coordinates (r, φ, z), introducing vector ξ with coordinates (a, φ, z), where a is SWCNT radius, φ —

azimuthal angle, and z — linear coordinate calculated along the nanotube axis.

Using the linearized continuity equation

$$\frac{\partial n(\xi,t)}{\partial t} + n_0 \nabla \cdot \mathbf{u}(\xi,t) = 0 \tag{1}$$

and linearized motion equation

$$\frac{\partial \mathbf{u}(\xi,t)}{\partial t} = -\frac{e}{m_{\text{eff}}}\mathbf{E}_{\|}(\xi,t) - \frac{\alpha}{n_0}\nabla n(\xi,t) - \frac{\mathbf{u}(\xi,t)}{\tau}, \tag{2}$$

where $\mathbf{u}(\xi,t)$, n_0 and $n(\xi,t)$ — the velocity, equilibrium and perturbed surface densities (surface concentrations) of electrons on the nanotube wall, respectively, $\mathbf{E}_{\|}(\xi,t)$ — tangential (with respect to the nanotube wall) component of the SPP electric field, τ — relaxation constant, e and m_{eff} — charge and effective mass of the electron [27,28]. In equation (2) the notation $\alpha = V_{\text{F}}^2/2$ stands for the square of the wave propagation velocity in a homogeneous electron fluid, where V_{F} is the electron Fermi velocity. The first term on the right side of equation (2) is the force acting on valence electrons from the tangential electric field component, the second corresponds to the internal interaction force in the electron fluid related to surface electron density perturbations. The third term accounts for collisional losses characterized by τ.

Eliminating $n(\xi,t)$ from equations (1) and (2), one can obtain the conductivity tensor for the SWCNT wall $\hat{\sigma}$, which defines the surface current density $\mathbf{j}_{\text{s}} = \hat{\sigma}\mathbf{E}_{\|}$, where $\mathbf{E}_{\|} = E_z\mathbf{e}_z + E_\varphi\mathbf{e}_\varphi$. The tensor components have the following form:

$$\begin{aligned}
\sigma_{zz}^m &= \sigma_0\Omega^{-1}(\omega\tilde{\omega} - \alpha m^2/a^2),\\
\sigma_{z\varphi}^m &= \sigma_{\varphi z}^m = \sigma_0\Omega^{-1}\alpha\beta m/a,\\
\sigma_{\varphi\varphi}^m &= \sigma_0\Omega^{-1}(\omega\tilde{\omega} - \alpha\beta^2),
\end{aligned} \tag{3}$$

where $\sigma_0 = in_0e^2/(m_{\text{eff}}\tilde{\omega})$, $\Omega = \omega\tilde{\omega} - \alpha(\beta^2 + m^2/a^2)$, $\tilde{\omega} = \omega + i\tau^{-1}$, β is the propagation constant of the SPP, $m = 0, 1, 2\ldots$ is the azimuthal mode number. This model takes into account spatial dispersion of SPPs, as well as the azimuthal component of current on the nanotube wall.

It should be noted that relations (3) have a similar form to CNT conductivity formulas for intraband transitions of π electrons obtained by semiclassical models. The frequency boundary of optical interband transitions usually lies in the mid-infrared range [1,5]. Features of formulas (3) are related to the following factors:

– Size effects are taken into account, manifested in the dependence of the dynamic conductivity on the radius of curvature of the SWCNT wall,

– Both radial and azimuthal components of the surface current density on the SWCNT wall are taken into account,

– Dependence of the conductivity tensor components on the azimuthal mode number m is included.

Dispersion Relation for SPPs in Single SWCNT:

Solving Maxwell's equations in cylindrical coordinates, one can write the Helmholtz equation for the longitudinal E_z electric field component at a distance r from the SWCNT axis:

$$\frac{d^2E_z}{dr^2} + \frac{1}{r}\frac{dE_z}{dr} - \left(\kappa^2 + \frac{m^2}{r^2}\right)E_z = 0, \tag{4}$$

where $\kappa^2 = \beta^2 - \omega^2/c^2$, c is the speed of light in vacuum. A similar equation can be written for the longitudinal magnetic field by replacing E_z with H_z. The transverse $(E_{r,\varphi}, H_{r,\varphi})$ and longitudinal (E_z, H_z) components of the wave fields are related by:

$$E_r = -\frac{\beta}{\kappa^2}\frac{dE_z}{dr} + \frac{m\omega\mu_0}{r\kappa^2}H_z, \quad E_\varphi = \frac{\beta m}{r\kappa^2}E_z + \frac{i\omega\mu_0}{\kappa^2}\frac{dH_z}{dr}, \tag{5}$$

$$H_r = -\frac{\beta}{\kappa^2}\frac{dH_z}{dr} + \frac{m\omega\varepsilon_0}{r\kappa^2}E_z, \quad H_\varphi = \frac{\beta m}{r\kappa^2}H_z + \frac{i\omega\varepsilon_0}{\kappa^2}\frac{dE_z}{dr}, \tag{6}$$

where μ_0 and ε_0 are the magnetic permeability and dielectric permittivity of vacuum. To solve the Helmholtz equation (4), boundary conditions for wave fields on the nanotube wall $(r = a)$ must be considered, including continuity conditions of tangential electric field components:

$$\begin{aligned}
E_z(a)|_{r=-a} &= E_z(a)|_{r=+a},\\
E_\varphi(a)|_{r=-a} &= E_\varphi(a_j)|_{r=+a},
\end{aligned} \tag{7}$$

and conditions for tangential magnetic field components:

$$H_z(a)|_{r=+a} - H_z(a)|_{r=-a} = -\sigma_{\varphi z}E_z - \sigma_{\varphi\varphi}E_\varphi, \tag{8}$$

The resulting determinant equation determines the dispersion relation $\beta(\omega, m) = 0$ for SPP modes,

$$\begin{vmatrix}
I_m(\kappa a) & \frac{m\beta}{\kappa^2 a}I_m(\kappa a) & -I_m(\kappa a)\Pi_1 & \frac{i\omega\varepsilon_0 I_m'(\kappa a)}{\kappa}\times I_m(\kappa a)\Pi_2\\
-K_m(\kappa a) & -\frac{m\beta}{\kappa^2 a}K_m(\kappa a) & 0 & -\frac{i\omega\varepsilon_0 K_m'(\kappa a)}{kappa}\\
0 & \frac{i\omega\mu_0 I_m'(\kappa a)}{\kappa} & I_m(\kappa a) & -\frac{m\beta}{\kappa^2 a}I_m(\kappa a)\\
 & & -\frac{i\omega\mu_0\sigma_{\phi\phi}^m I_m'(\kappa a)}{\kappa} & -\frac{i\omega\mu_0\sigma_{z\phi}^m I_m'(\kappa a)}{\kappa}\\
0 & -\frac{i\omega\mu_0 K_m'(\kappa a)}{\kappa} & -K_m(\kappa a) & \frac{m\beta}{\kappa^2 a}K_m(\kappa a)
\end{vmatrix} = 0, \tag{9}$$

where I_m and K_m are modified Bessel functions of m order, and parameters $\Pi_1 = \sigma_{z\phi}^m + \sigma_{\phi\phi}^m\frac{m\beta}{a\kappa^2}$, $\Pi_2 = \sigma_{zz}^m + \sigma_{z\phi}^m\frac{m\beta}{a\kappa^2}$.

Analysis and Discussion

Analysis of the dispersion properties of SPP modes of different orders m in SWCNTs is conducted by numerically solving the determinant equation (9). To estimate the ratio of equilibrium concentration of electrons to the effective electron mass, we use the formula provided

Table 1. Chirality indices and corresponding chirality angles and radii of metallic SWNTs

Radius of SWNT, nm	Index N	Index M	Chirality angle, deg
0.489	10	4	16.1
1.996	51	0	0
1.998	50	2	1.9
2.001	49	4	3.9
1.998	38	20	19.8
2.001	31	28	28.3
4.997	124	7	2.7
5.0002	123	9	3.5
4.999	114	24	9.4
5.0002	108	33	12.9
4.999	91	55	21.9
5.0002	84	63	25.3

in [28]: $n_0/m_{\text{eff}} = 2V_{\text{E}}/\pi^2\hbar a$, where the Fermi velocity is $V_{\text{F}} = 10^6$ m/s. For convenience in presenting the dispersion dependencies, normalized parameters for the propagation constant (PC) and frequency are introduced respectively as: $a_0 = 1$ nm and $\omega_0 = \frac{e}{\pi a_0}\sqrt{\frac{2V_{\text{F}}}{\varepsilon_0 h}} \approx 2.36 \cdot 10^{15}\,\text{s}^{-1}$.

The conductivity type of the SWCNT is defined by chirality indices (N, M), which are related to the SWCNT radius by the relation [3,29]

$$a = \sqrt{M^2 + N^2 + MN}\,\frac{\sqrt{3}d_0}{2\pi}, \qquad (10)$$

where $d_0 = 0.142$ nm is the distance between neighboring carbon atoms in the graphite plane. In this work, we consider metallic SWCNTs with three radii, taking them in calculations as 0.5, 2 and 5 nm. The chirality indices and more precise corresponding radii calculated by the above relation (10), are given in the Table 1. The difference between exact radii and rounded values used in calculations is insignificant (less than 0.1 nm) and does not noticeably affect numerical results. Note that one fixed radius for analysis can correspond to multiple pairs of chirality indices (N, M) (see the Table 1).

Figure 1 shows the dependence of reduced propagation constant ω/ω_0 for SPP modes in isolated SWCNTs with radius 0.5 nm. Here and below, the loss level $\tau = 10^{-12}$ s is chosen close to that given in [1,30,31]. One can see that for each mode with index $m > 0$ here exists a cutoff frequency region. The cutoff regime $(\beta''/\beta' \geq 1)$ corresponds to high imaginary parts $(\beta'' > 10^9\,\text{m}^{-1})$ and relatively low real parts $(\beta' < 3 \cdot 10^8\,\text{m}^{-1})$ of the propagation constant. The imaginary part of the PC $1/\beta''$ defines the propagation length of the SPPs, with a maximum value not less than $1\,\mu$m in the considered spectral range, increasing as frequency decreases. The presence of multiple branches of dispersion curves indicates the possibility of excitation of several surface waves simultaneously at the same frequency in the SWCNT, differing by their field distribution cross-section, SPP wavelength $(\lambda_{SPP} = \frac{2\pi}{\beta'})$ and propagation length.

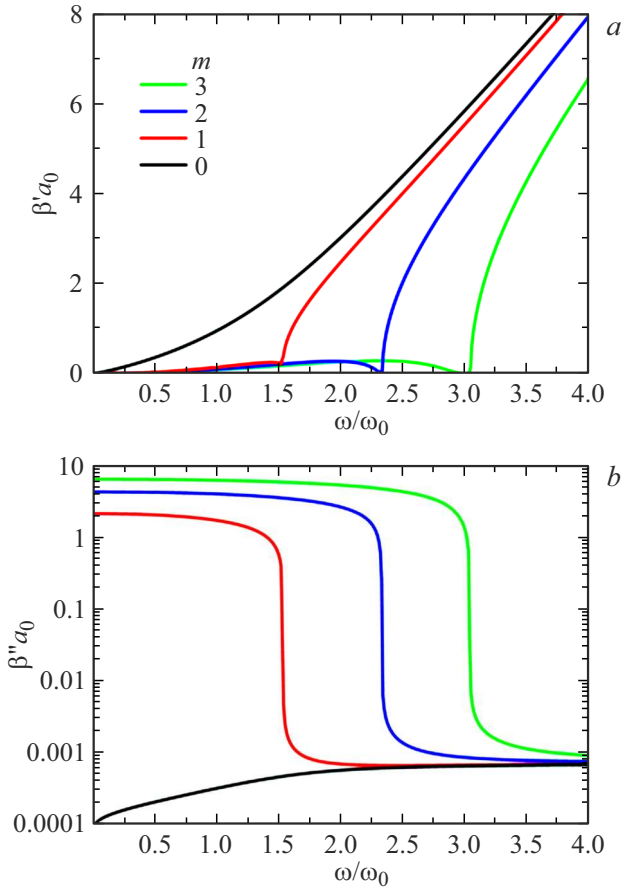

Figure 1. Dispersion dependences for the real (a) and imaginary (b) parts of the reduced PC for the first four SPP modes in SWCNTs of radius $a = 0.5$ nm.

An important parameter of SPPs excited in the nanotube is the slowing-down factor defined as the ratio of the speed of light to the phase velocity of the surface plasmon-polariton:

$$K_{\text{dec}} = c/V_{\text{ph}} = \beta' c/\omega. \qquad (11)$$

High values of K_{dec} enable phase velocity matching of SPP modes to the drift velocity of the direct current pump, which is significant for developing and creating terahertz amplifiers and generators [11,12,18]. The analysis shows that higher-order SPP modes $(m > 0)$ have higher propagation losses and lower slowing-down factors K_{dec} compared to the fundamental mode $m = 0$. Therefore, subsequently, we consider the frequency range up to $0.4\omega_0$, where only the fundamental mode exists. In this frequency range, SPP propagation length can reach up to $10\,\mu$m.

Figure 2 depicts the dependencies of reduced propagation constant and slowing-down factor on reduced frequency for the fundamental SPP mode in isolated SWCNTs of various radii within the frequency range $\omega = (0.01{-}0.4)\omega_0$. It is seen that increasing frequency increases both the real and

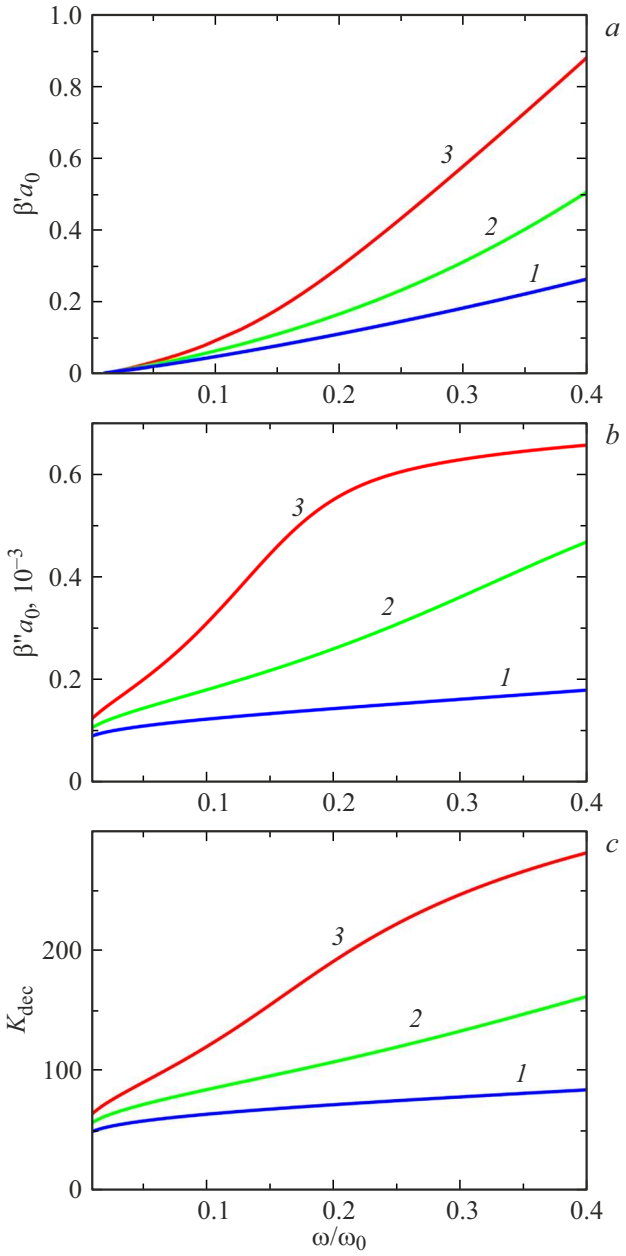

Figure 2. Dispersion dependences for the real (a) and imaginary (b) parts of the reduced PC for the fundamental SPP mode in isolated SWCNTs of radius $a = 0.5$, 2, 5 nm (curves *1, 2, 3*).

imaginary parts of the propagation constant and the slowing-down factor for SWCNTs of all radii. For larger radius nanotubes, both propagation constant components and slowing-down factors of SPPs are higher. The main trend is that the larger the tube radius, the higher the slowing-down factor at the same frequencies. For example, in small diameter nanotubes ($a = 0.5$ nm) the slowing-down factor does not exceed 85, while in medium diameter ($a = 2$ nm) and large diameter ($a = 5$ nm) nanotubes, it exceeds 160 and 280, respectively. The SPP phase velocity becomes at least 100 times less than the speed of electromagnetic waves in vacuum at frequencies starting from $0.2\omega_0$ and $0.1\omega_0$ for medium diameter and large diameter SWCNTs, respectively.

The dispersion properties of SPPs in SWCNT arrays were analyzed using Comsol Multiphysics finite element modeling solving Helmholtz's equation for the conductivity tensor defined by expressions (3). The considered arrays are infinite ordered arrays with square unit cells where nearest nanotube centers are spaced by distance d (array period). Fig. 3 shows the dependences of the complex reduced PC and the slowing down coefficient on the array period d for the SPPs of different frequencies in small and large diameter nanotubes with radii of $a = 0.5$ and 5 nm respectively. The simulation was performed using the finite element method for a 2D square-shaped domain containing a single nanotube, using periodic boundary conditions. Insert in Figure 3a shows the electric field intensity distribution of the fundamental mode in the modeled area. Rectangular areas on all panels of Figure 3 denote forbidden ranges ($d < 2a$), where the walls of neighboring SWCNTs overlap. For sparse arrays ($d \gg 2a$) for both radii (0.5 and 5 nm) the propagation constant of the fundamental mode practically does not depend on period d. In this case, SPPs in nanotubes interact weakly, and their propagation constants are equal to those of isolated SWCNTs. In dense arrays where period d is less than $2(a + \Delta)$ with $\Delta \approx 2/\beta''$ the scale of evanescent field decay outside the nanotube, the dispersion characteristics become sensitive to changes in nanotube spacing. Because propagation constants β in large diameter SWCNTs are higher at all frequencies, in accordance with $\Delta \approx 2/\beta'$ their SPP dispersion depends on array density for smaller relative distances d/a (Fig. 3, *d, e, f*) compared to small diameter nanotubes (Fig. 3, *a, b, c*). Increasing array density reduces the real part of the propagation constant (Fig. 3, *a* and *d*) and increases dissipative losses (Fig. 3, *b* and *e*). Reduction of propagation constant raises phase velocity and decreases slowing-down factor (Fig. 3, *c* and *f*). Overall, arrays of large diameter SWCNTs are preferable for achieving high slowing-down factors.

Figure 4 shows dispersion dependencies of complex reduced propagation constant for the fundamental mode for different array periods and nanotube radii. In isolated nanotubes ($d \to \infty$, dashed lines) cutoff of the fundamental mode is absent and dispersion is nearly linear. In dense arrays ($d = 11$ nm), the mode cutoff occurs at frequencies below $0.25\omega_0$. Furthermore, near the cutoff, the frequency dependence of the real part of the permittivity significantly deviates from linearity, regardless of the SWCNT radius (curves *2, 3* in Fig. 4, *a* and Fig. 4, *c*). The dispersion characteristics of SPPs in isolated SWCNTs and sparse arrays of SWCNTs at $d > 20$ nm coincide closely over the frequency range $\omega > 0.3\omega_0$ (curves *1* and *2* in Fig. 4, *a* and *c*). Therefore, dispersion characteristics of SPPs in SWCNT arrays within this range practically match those of an isolated nanotube.

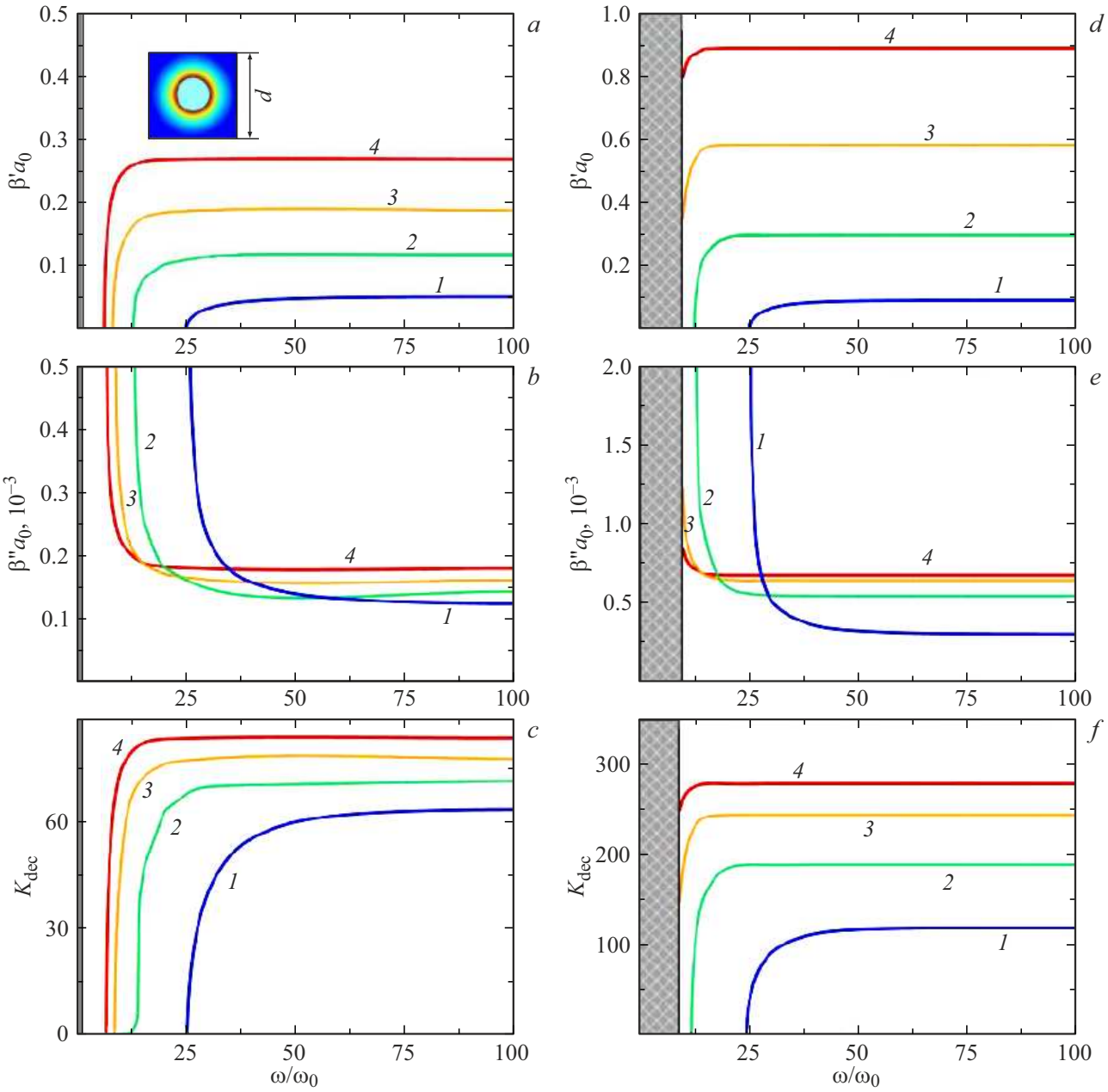

Figure 3. Dependences of the real (*a* and *d*) and imaginary (*b* and *e*) parts of the reduced PC, as well as the slowing down coefficient (*c* and *f*) on the period *d* of the SWCNT array for the fundamental SPP mode. Curves *1, 2, 3, 4* correspond to frequencies 0.1, 0.2, 0.3 and 0.4. Radii of SWNTs $a = 0.5$ (*a*, *b* and *c*) and 5 nm (*d, e* and *f*).

Conclusion

In the present work, using the hydrodynamic approach, the dispersion characteristics of SPPs in isolated SWCNTs of different radii (from 0.5 to 5 nm) and ordered arrays based on them are studied. The analysis is performed in the terahertz and far-infrared ranges. It is shown that SPPs in an SWCNT array with period $d > 2(a + 2/\beta') > 20$ nm are virtually identical in their dispersion properties from SPPs in isolated nanotubes. The interaction of plasmonic evanescent fields of nanotubes in a dense array leads to a reduction of the propagation constant, an increase in the SPP propagation length, and the appearance of a cutoff for the fundamental mode.

It is found that in array-forming nanotubes of small radii, the slowing-down factor of SPPs for mode with $m = 0$ does not exceed 100. For SWCNT arrays with radii above 2 nm at frequencies around 40 THz and higher, the slowing-down factor can reach higher values. The results may be useful in the development of compact sensors, amplifiers, and SPP generators based on ordered arrays of carbon nanotubes.

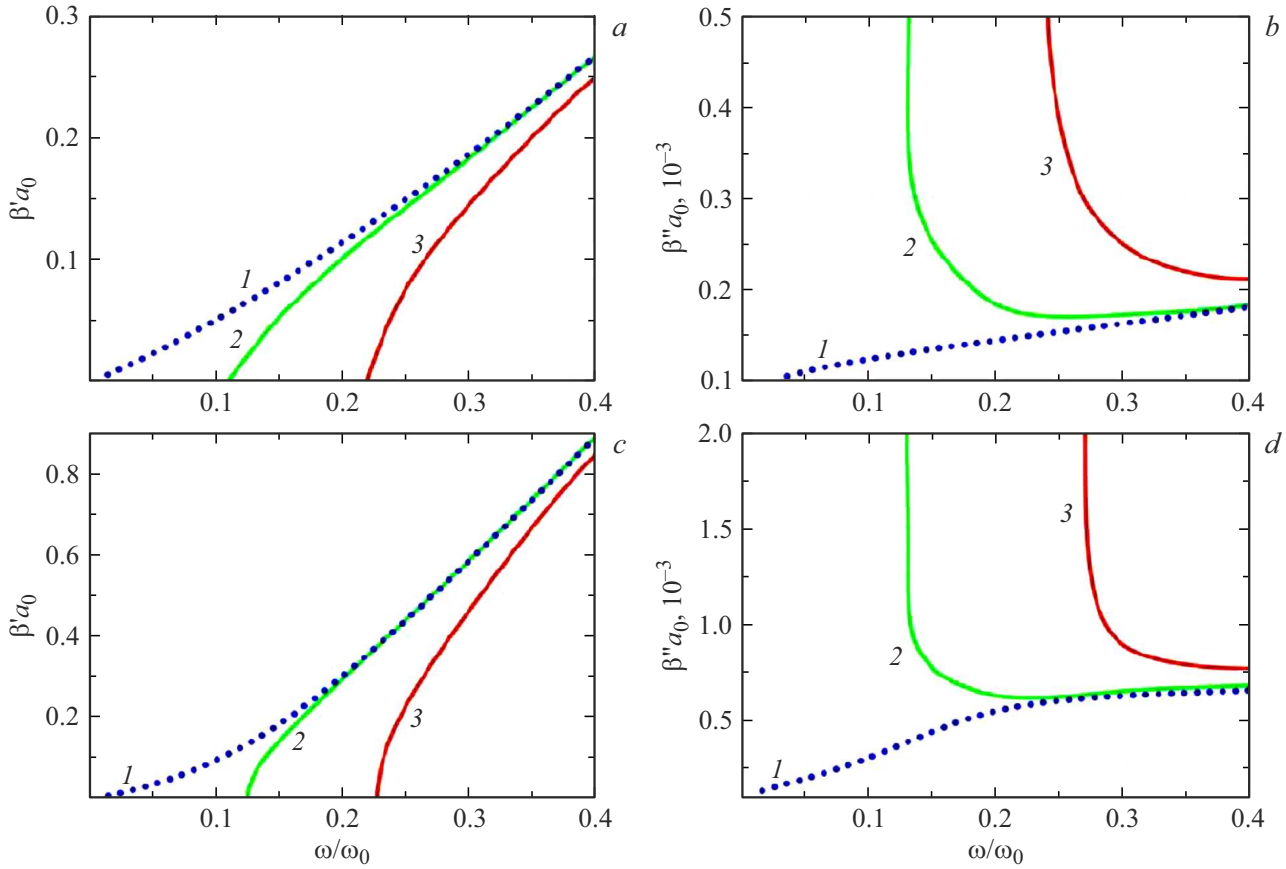

Figure 4. Dependences of the real (*a* and *c*) and imaginary (*b* and *d*) parts of the reduced PC on the reduced frequency for different periods of the *d* array and radii of the SWCNT for the fundamental SPP mode. Curves *1, 2, 3* correspond to the values of the period $d = \infty$, 20 and 11 nm. Radii of SWNTs $a = 0.5$ (*a* and *b*) and 5 nm (*c* and *d*).

Funding

This work was supported by the Russian Science Foundation (grant No. 23-19-00880).

Conflict of interest

The authors declare that they have no conflict of interest.

References

[1] G.Y. Slepyan, S.A. Maksimenko, A. Lakhtakia, O. Yevtushenko, A.V. Gusakov. Phys. Rev. B, **60** (24), 17136 (1999). DOI: 10.1103/PhysRevB.60.17136

[2] A.V. Eletskii. Physics-Uspekhi, **52** (3), 209(2009). DOI: 10.3367/UFNE.0179.200903A.0225.

[3] P.N. D'yachkov, *Uglerodnye nanotrubki: stroenie, svoistva, primeneniya* (Binom. Laboratoriya znanij, M. 211). (in Russian)

[4] S. Rathinavel, K. Priyadharshini, D. Panda. Mater. Sci. Eng. B, **268**, 115095 (2021). DOI: 10.1016/j.mseb.2021.115095

[5] M.G. Burdanova, A.P. Tsapenko, M.V. Kharlamova, E.I. Kauppinen, B.P. Gorshunov, J. Kono, J. Lloyd-Hughes. Adv. Opt. Mater., **9** (24), 2101042 (2021). DOI: 10.1002/ADOM.202101042

[6] K.G. Batrakov, O.V. Kibis, P.P. Kuzhir, M.R. da Costa, M.E. Portnoi. J. Nanophotonics, **4** (1), 041665 (2010). DOI: 10.1117/1.3436585

[7] A. Moradi. J. Electromagn. Anal. Appl., **2** (12), 672 (2010). DOI: 10.4236/JEMAA.2010.212088

[8] A. Moradi. Photonics Nanostructures — Fundam. Appl., **11** (1), 85 (2013). DOI: 10.1016/j.photonics.2012.09.001

[9] L. Martín-Moreno, F.J.G. De Abajo, F.J. García-Vidal. Phys. Rev. Lett., **115** (17), 173601 (2015). DOI: 10.1103/PHYSREVLETT.115.173601

[10] S.A. Afanas'ev, V.A. Zajcev, S.G. Moiseev, I.A. Rozhlejs, D.G. Sannikov, G.V. Tertyshnikova. Semicon., **58** (9), 467 (2024). DOI: 10.61011/SC.2024.09.59910.6326A

[11] A.S. Kadochkin, S.G. Moiseev, Y.S. Dadoenkova, V.V. Svetukhin, I.O. Zolotovskii. Opt. Express, **25** (22), 27165 (2017). DOI: 10.1364/oe.25.027165

[12] A.S. Kadochkin, S. Moiseev, Y.S. Dadoenkova, F. Bentivegna, V. Svetukhin, I.O. Zolotovsky. J. Opt., **22**, 12, 125002 (2020). DOI: 10.1088/2040-8986/abb8c4

[13] V. Perebeinos, J. Tersoff, P. Avouris. Phys. Rev. Lett., **94** (8), 086802 (2005). DOI: 10.1103/PHYSREVLETT.94.086802

[14] K. Liu, J. Deslippe, F. Xiao, R.B. Capaz, X. Hong, S. Aloni, A. Zettl, W. Wang, X. Bai, S.G. Louie, E. Wang, F. Wang. Nat. Nanotechnol., **7** (5), 325 (2012). DOI: 10.1038/NNANO.2012.52

[15] D.A. Svintsov, A.V. Arsenin, D.Yu. Fedyanin, A. Kriesch, S.P. Burgos, D. Ploss, H. Pfeifer, H.A. Atwater, U. Peschel, I. Vurgaftman, M. Kim, J. Meyer, A. Mäkinen, K. Bussmann, L. Cheng, F. Choa, J. Long, A.W. Fang, R. Jones, H. Park, O. Cohen, O. Raday, M.J. Paniccia, J.E. Bowers. Opt. Express, **23** (15), 19358 (2015). DOI: 10.1364/OE.23.019358
[16] S.G. Moiseev, Y.S. Dadoenkova, A.S. Kadochkin, A.A. Fotiadi, V.V. Svetukhin, I.O. Zolotovskii. Ann. Phys., **530** (11), 1800197 (2018). DOI: 10.1002/andp.201800197
[17] T.A. Morgado, M.G. Silveirinha. ACS Photonics, **5** (11), 4253 (2018). DOI: 10.1021/ACSPHOTONICS.8B00987
[18] S.A. Afanas'ev, A.A. Fotiadi, A.S. Kadochkin, E.P. Kitsyuk, S.G. Moiseev, D.G. Sannikov, V.V. Svetukhin, Y.P. Shaman, I.O. Zolotovskii. Photonics, **10** (12), 1317 (2023). DOI: 10.3390/PHOTONICS10121317
[19] P. Longe, S.M. Bose. Phys. Rev. B, **48** (24), 18239 (1993). DOI: 10.1201/9781351121996-7
[20] S.A. Maksimenko, G.Y. Slepyan, G.Y. Slepyan. In: *Electromagnetic Fields Unconv. Struct. Mater*, ed. by N. Singh Onkar, A. Lakhtakia (John Wiley & Sons, Inc., New York, 2000), pp. 217–255.
[21] A. Moradi. J. Appl. Phys., **122** (13), 133103 (2017). DOI: 10.1063/1.4997454
[22] A. Moradi, H. Khosravi. Phys. Rev. B – Condens. Matter Mater. Phys., **76** (11), 113411 (2007). DOI: 10.1103/PHYSREVB.76.113411
[23] D.J. Mowbray, Z.L. Mišković, F.O. Goodman. Phys. Rev. B – Condens. Matter Mater. Phys., **74** (19), 1 (2006). DOI: 10.1103/PhysRevB.74.195435
[24] T. Stöckli, J.M. Bonard, A. Châtelain, Z.L. Wang, P. Stadelmann. Phys. Rev. B, **64** (11), 115424 (2001). DOI: 10.1103/PhysRevB.64.115424
[25] C. Yannouleas, E.N. Bogachek, U. Landman. Phys. Rev. B, **53** (15), 10225 (1996). DOI: 10.1103/PhysRevB.53.10225
[26] G. Chen, S. Sakurai, M. Yumura, K. Hata, D.N. Futaba. Carbon N. Y., **107**, 433 (2016). DOI: 10.1016/j.carbon.2016.06.024
[27] A. Moradi. Phys. Lett. Sect. A Gen. At. Solid State Phys., **372** (34), 5614 (2008). DOI: 10.1016/j.physleta.2008.06.071
[28] G. Miano, F. Villone. IEEE Trans. Antennas Propag., **54** (10), 2713 (2006). DOI: 10.1109/TAP.2006.882170
[29] A.V. Eletskii. Physics–Uspekhi, **45** (4), 369(2002). DOI: 10.1070/PU2002v045n04ABEH001033.
[30] Y. Miyamoto, S.G. Louie, M.L. Cohen. Phys. Rev. Lett., **76** (12), 2121 (1996). DOI: 10.1103/PhysRevLett.76.2121
[31] R.A. Jishi, M.S. Dresselhaus, G. Dresselhaus. Phys. Rev. B, **47** (24), 16671 (1993). DOI: 10.1103/PhysRevB.47.16671

Translated by J.Savelyeva